*Int. J. Multiphase Flow* Vol. 18, No. 2, pp. 217–227, 1992
Printed in Great Britain. 

0301-9322/92 $5.00 + 0.00


# THEORETICAL AND EXPERIMENTAL STUDY OF THE ONSET OF LIQUID ENTRAINMENT DURING DUAL DISCHARGE FROM LARGE RESERVOIRS

K. F. ARMSTRONG,[1] S. D. PARROTT,[1,2] G. E. SIMS,[1] H. M. SOLIMAN[1] and V. S. KRISHNAN[2]†

[1]Department of Mechanical and Industrial Engineering, University of Manitoba, Winnipeg, Manitoba, Canada R3T 2N2

[2]Thermalhydraulics Branch, Whiteshell Laboratories, AECL Research, Pinawa, Manitoba, Canada R0E 1L0

*(Received 20 February 1991; in revised form 16 September 1991)*

**Abstract**—The phenomenon of liquid entrainment is investigated experimentally and theoretically for the condition of simultaneous discharge from two small orifices located on the side of a high-pressure reservoir containing stratified layers of two immiscible fluids. The measured critical height for air–water layers is found to be a function of the two discharge rates and the vertical distance separating the centrelines of the orifices. An independent theoretical analysis is conducted which gives good agreement with the experimental data.

*Key Words:* liquid entrainment, dual discharge, experiment, theory

## 1. INTRODUCTION

Significant research efforts have been directed recently towards the problem of two-phase flow through small breaks in horizontal pipes under stratified-flow conditions. Results of this research are relevant to the development of reactor safety codes for the analysis of postulated loss-of-coolant accidents (LOCA). Zuber (1980) pointed out that the mass flow rate and quality of the discharge through small breaks can be strongly influenced by the phenomena of liquid entrainment and gas pull-through. Recent studies have succeeded in developing correlations for the onsets of these two phenomena for the case of a single break located at the top, bottom or side of a horizontal pipe (Crowley & Rothe 1981; Smoglie & Reimann 1986; Schrock *et al.* 1986; Smoglie *et al.* 1987; Micaelli & Memponteil 1989).

In some practical situations, multiple discharge may take place simultaneously from several orifices at the same pipe cross-section. An example of these situations is a horizontal manifold similar to a flow distribution header in a CANDU nuclear reactor heat transport system. Each header is connected to the fuel channels by banks of five feeders located at successive cross-sections of the header. In a recent investigation, Parrott *et al.* (1991) reported a basic experiment which constitutes a first step towards understanding the flow distribution in such complex systems under LOCA conditions. That experiment was successful in developing empirical correlations for the onset of gas pull-through during discharge from a large reservoir through two side orifices separated by variable vertical distances. The present investigation provides experimental data and theoretical analysis for the onset of liquid entrainment under geometrical and flow conditions similar to those of Parrott *et al.* (1991).

## 2. EXPERIMENTAL INVESTIGATION

### 2.1. Experimental parameters

The relevant geometrical and flow parameters for the present experiment are shown schematically in figure 1. Two small orifices of equal diameter $d$ are placed on the side of a large reservoir

† Current address: Analysis and Design, AECL CANDU, Mississauga, Ontario, Canada L5K 1B2.

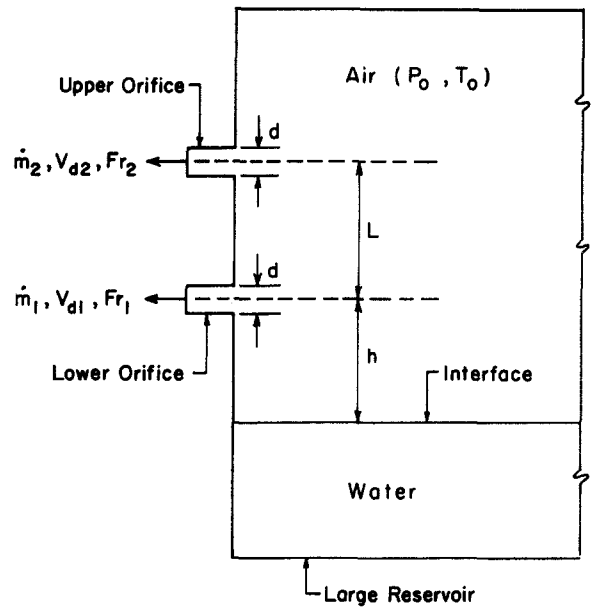


Figure 1. Geometry and experimental parameters.

separated by a vertical distance $L$ centre-to-centre. The air inside the reservoir is at a stagnation pressure $P_0$ and stagnation temperature $T_0$. Controllable amounts of air are withdrawn with mass flow rates $\dot{m}_1$ and $\dot{m}_2$ from the lower and upper orifices, respectively. The corresponding values of the Froude number, $Fr_1$ and $Fr_2$, can be determined from the following definition:

$$Fr = \frac{V_d}{\sqrt{gd\dfrac{\Delta\rho}{\rho}}}, \qquad [1]$$

where the mean discharge velocity $V_d$ is given by

$$V_d = \frac{\dot{m}}{\dfrac{\pi}{4}\rho d^2}, \qquad [2]$$

$g$ is the gravitational acceleration, $\rho$ is the air density at the inlet of the orifice and $\Delta\rho$ is the water–air density difference. For given values of $Fr_1$, $Fr_2$, $L$ and $d$, there is a critical height $h$ at which liquid entrainment begins to take place. The main objective of this experiment, and the analysis presented later, is to determine the influences of $L$ and $Fr_2$ on the value of $h$.

Following Parrott *et al.* (1991) and neglecting the effects of viscosity and surface tension, we can perform a dimensional analysis with $h$, $L$, $d$, $g\,\Delta\rho/\rho$, $V_{d1}$ and $V_{d2}$ as the relevant physical quantities. The inclusion of $g\,\Delta\rho/\rho$ as a single physical quantity follows from Craya's (1949) reasoning. Such an analysis would yield the following dimensionless groups: $h/d$, $L/d$, $Fr_1$ and $Fr_2$. Therefore, the correlation for the onset of liquid entrainment would be expected to take the form

$$\frac{h}{d} = f\left(Fr_1, Fr_2, \frac{L}{d}\right). \qquad [3]$$

Guided by [3], the experiment was conducted such that values of $h$ were measured over a wide range of $Fr_1$ using a number of combinations of $Fr_2$ and L/d. The theoretical analysis, which simulates the orifices as point sinks, results in a considerable simplification over [3], as will be seen later.

### *2.2. Experimental apparatus*

Figure 2 shows a schematic diagram of the flow loop. The test section was connected to an air supply with a pressure regulator which maintained a steady pressure of about 310 kPa throughout

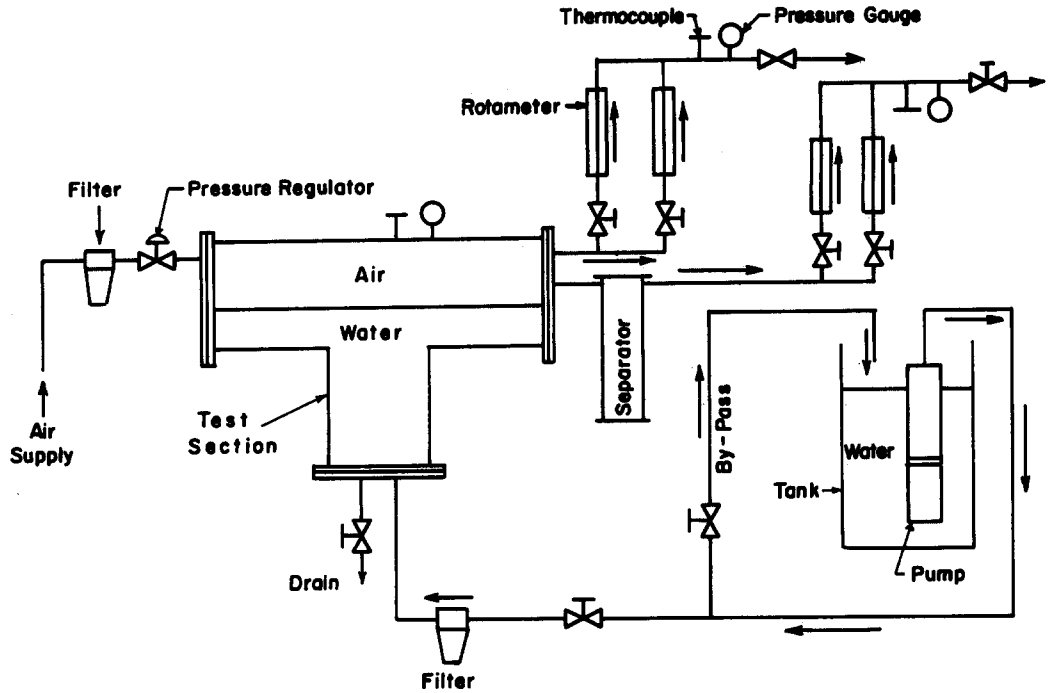


Figure 2. Schematic diagram of the experimental apparatus.

the experiment. The incoming air was fed into the test section via a dispersion box for the purpose of eliminating any surface waves or ripples due to jetting. A submersible circulating pump supplied distilled water to the test section at a rate regulated by a throttling valve and a by-pass line. The rate of discharge of air from the test section through each of the two outlet orifices was measured by two air rotameters with overlapping ranges. The maximum capacities of the rotameters on each outlet line were 63 and 730 standard litres/min. The rate of discharge through each orifice was controlled by throttling valves upstream and downstream of the rotameters. A centrifugal-type separator was installed on the line connected to the lower orifice (where liquid entrainment occurred), in order to prevent any liquid droplets from reaching the air rotameters. Discharged air was finally exhausted to the atmosphere.

The temperature and pressure of air within the test section, $T_0$ and $P_0$, respectively, were measured during the experiment. Temperature and pressure readings were also recorded at the outlet of each rotameter from which the density was calculated and, together with the measured volumetric flow rate, made possible the evaluation of air mass flow rates.

Details of the test-section design were reported by Parrott *et al.* (1991). The discharge orifices were holes, 6.35 mm dia and 127 mm long (i.e. 20 diameters), machined in a brass block which was bolted to the outlet flange. A surveying transit was used to ensure that the faces of the flange and the block were vertical and that the centrelines of the orifices fell on a straight vertical line. The liquid height in the test section (from which values of $h$ were determined) was measured by a differential pressure transducer connected to pressure taps on the air and water sides. All thermocouples, pressure gauges and the differential pressure transducer were calibrated before testing began while the manufacturer's calibration was used for the air rotameters.

### *2.3. Experimental procedure*

Liquid entrainment involves the sudden formation of a small liquid stream that travels on the surface of the brass block vertically upwards towards the lower orifice. Some early observations indicated that for the same operating conditions ($Fr_1$, $Fr_2$, $L$) the value of the critical height $h$ could be influenced by whether the brass block was wet or dry before the test; however, detection of the phenomenon was difficult with a wet surface. Since it is difficult to characterize surface wetness in a quantitative manner, and considering the detection problem, it was decided to perform all

the present tests with the condition whereby the brass surface between the gas–liquid interface and the lower orifice was dry before any test.

Another consideration was the cleanliness of the brass block surface. This was held relatively consistent by cleaning the brass block surface several times throughout the investigation.

The following procedure was followed for each datum point:

1. Distilled water was pumped into the test section to a level well below the lower orifice and air pressure was applied and maintained steady at approx. 310 kPa.
2. Air flow through the outlet orifices was initiated at a high flow rate in order to dry the face of the brass block (if wet). When dry conditions had been achieved, the two air flows were then regulated to the desired values of $Fr_1$ and $Fr_2$. Readings of the rotameters, as well as the pressure and temperature within the test section and downstream from the rotameters were recorded.
3. The water level in the test section was increased very slowly (at a rate of about 1.5 mm/min). As the critical height was approached, an upward deformation of the gas–liquid interface occurred beneath the orifices. When the critical height was reached, a small stream of water suddenly formed between the deformed interface and the lower orifice. This incidence was detected visually through the transparent part of the test section and the corresponding reading of the pressure transducer (from which $h$ was evaluated) was immediately recorded.

### 2.4. Data reduction

The recorded data for each test run included the mass flow rates $\dot{m}_1$ and $\dot{m}_2$, the critical height $h$, and the stagnation conditions within the test section $P_0$ and $T_0$. Strictly speaking, there was some finite air velocity in the test section; however, the cross-sectional area was so large that this velocity was $<0.5$ m/s at the highest discharge rates. In order to determine $Fr_1$ and $Fr_2$, the inlet conditions at both orifices had to be determined. This was done by applying the following procedure for each orifice:

1. The air was treated as an ideal gas and an energy balance was applied between the stagnation conditions and the orifice inlet, thus giving

$$c_p T_0 = c_p T + \frac{V_d^2}{2}, \qquad [4]$$

where $c_p$ is the constant-pressure specific heat and $T$ is the temperature at orifice inlet.

2. From mass conservation, we have

$$\dot{m} = \frac{\pi}{4} \rho d^2 V_d, \qquad [5]$$

where the density $\rho$ is given by

$$\rho = \frac{P}{RT}, \qquad [6]$$

$P$ is the pressure at orifice inlet and R is the ideal gas constant for air.

3. The expansion from stagnation conditions to orifice inlet was assumed to be isentropic, thus

$$T/T_0 = (P/P_0)^{(k-1)/k}, \qquad [7]$$

where $k$ is the ratio of specific heats.

Equations [4]–[7] were solved iteratively for the values of $P$, $T$, $\rho$ and $V_d$. Definition [1] was then used for the evaluation of Fr for each orifice.

The sensitivity of the results to the assumption of isentropic expansion was carefully assessed. It was found that this assumption has a small influence on the value of Fr, mainly because the differences $(T_0 - T)$ and $(P_0 - P)$ are small. For example, at a datum point corresponding to

the highest discharge rate, the isentropic assumption with $k = 1.4$ produces Fr = 30.66, while a polytropic expansion with $n = 2$ produces Fr = 29.99. Such deviation in Fr is small and it decreases further as the rate of discharge decreases.

### 2.5. *Experimental results*

The following ranges of geometrical and flow conditions were covered in this investigation:

$$P = 310 \text{ kPa (abs)},$$

$$d = 6.35 \text{ mm},$$

$$\frac{L}{d} = 1.5,\ 2,\ 3 \text{ and } 4,$$

$$\text{Fr}_1 = 1.7 \text{ to } 30$$

and

$$\text{Fr}_2 = 0 \text{ (condition of single discharge)}$$

$$= 8.23,\ 15.6,\ 23.4 \text{ and } 32.1 \left(\text{for } \frac{L}{d} = 1.5\right)$$

$$= 15.5 \text{ and } 31.5 \left(\text{for } \frac{L}{d} = 2,\ 3 \text{ and } 4\right).$$

Within the above conditions, liquid entrainment, as described earlier, occurred only at the lower orifice. The pattern described by Parrott *et al.* (1991) for gas pull-through, where the phenomenon occurred simultaneously at both orifices under certain operating conditions, was not observed in the present experiment.

The experimental results for the limiting condition of single discharge ($\text{Fr}_2 = 0$) are listed in table 1. Three sets of data were generated corresponding to approximately the same values of $\text{Fr}_1$ in order to check the repeatability of the results. Deviations among the three sets are small and, typically, any one of the sets is within $\pm 2\%$ from the mean. The closest set to the mean (typically within $\pm 0.5\%$) is set No. 3 and this segment of the results is presented in figure 3 along with Craya's (1949) correlation given by

$$\frac{h}{d} = 0.625\ \text{Fr}^{0.4}. \qquad [8]$$

The data are generally in good agreement with Craya's predictions. For $\text{Fr}_1 > 5$, figure 3 shows that the data follow the form of [8] with nearly the same exponent and about 6% deviation in the coefficient. At lower $\text{Fr}_1$, the data diverge slightly from the form of correlation [8]. This slight divergence is attributed to the fact that in deriving [8], the orifice was simulated by a point sink.

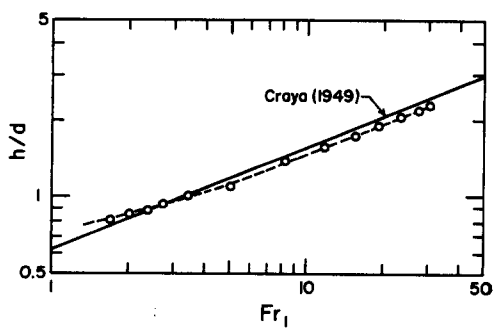


Figure 3. Data for single discharge ($\text{Fr}_2 = 0$).

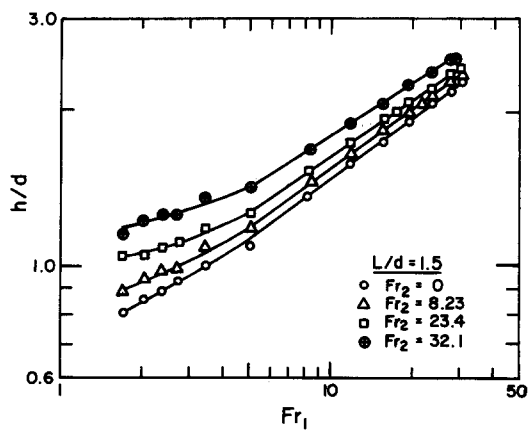


Figure 4. The influence of $\text{Fr}_2$ during dual discharge for $L/d = 1.5$.

Table 1. Experimental results for $Fr_2 = 0$

| Set No. 1 | | Set No. 2 | | Set No. 3 | |
|---|---|---|---|---|---|
| $Fr_1$ | $h/d$ | $Fr_1$ | $h/d$ | $Fr_1$ | $h/d$ |
| 29.8 | 2.24 | 30.7 | 2.31 | 30.5 | 2.29 |
| 27.3 | 2.16 | 27.8 | 2.23 | 27.8 | 2.20 |
| 23.4 | 2.03 | 23.3 | 2.08 | 23.4 | 2.07 |
| 19.2 | 1.89 | 19.4 | 1.94 | 19.3 | 1.91 |
| 15.4 | 1.72 | 15.6 | 1.77 | 15.5 | 1.75 |
| 11.7 | 1.53 | 11.8 | 1.59 | 11.7 | 1.56 |
| 8.24 | 1.29 | 8.27 | 1.38 | 8.25 | 1.37 |
| 5.17 | 1.07 | 5.19 | 1.12 | 5.03 | 1.09 |
| 3.40 | 0.96 | 3.52 | 1.05 | 3.44 | 1.00 |
| 2.78 | 0.85 | 2.79 | 0.91 | 2.75 | 0.93 |
| 2.41 | 0.88 | 2.42 | 0.93 | 2.39 | 0.89 |
| 2.06 | 0.85 | 2.06 | 0.87 | 2.04 | 0.85 |
| 1.71 | 0.75 | 1.68 | 0.83 | 1.71 | 0.80 |

Table 2. Experimental results for $Fr_2 > 0$

| $L/d = 1.5$ | | | | | | | | $L/d = 2$ | | | | $L/d = 3$ | | | | $L/d = 4$ | | | |
|---|---|---|---|---|---|---|---|---|---|---|---|---|---|---|---|---|---|---|---|
| $Fr_2 = 8.23$ | | $Fr_2 = 15.6$ | | $Fr_2 = 23.4$ | | $Fr_2 = 32.1$ | | $Fr_2 = 15.5$ | | $Fr_2 = 31.3$ | | $Fr_2 = 15.5$ | | $Fr_2 = 32.0$ | | $Fr_2 = 15.4$ | | $Fr_2 = 30.9$ | |
| $Fr_1$ | $h/d$ | $Fr_1$ | $h/d$ | $Fr_1$ | $h/d$ | $Fr_1$ | $h/d$ | $Fr_1$ | $h/d$ | $Fr_1$ | $h/d$ | $Fr_1$ | $h/d$ | $Fr_1$ | $h/d$ | $Fr_1$ | $h/d$ | $Fr_1$ | $h/d$ |
| 30.7 | 2.38 | 30.0 | 2.38 | 30.1 | 2.42 | 28.5 | 2.53 | 29.9 | 2.35 | 26.4 | 2.39 | 30.6 | 2.37 | 30.1 | 2.40 | 30.1 | 2.26 | 27.7 | 2.29 |
| 27.3 | 2.28 | 27.5 | 2.30 | 27.7 | 2.37 | 27.2 | 2.51 | 27.7 | 2.29 | 25.6 | 2.38 | 27.7 | 2.29 | 27.8 | 2.35 | 27.6 | 2.18 | 26.4 | 2.24 |
| 23.6 | 2.13 | 23.2 | 2.17 | 23.4 | 2.21 | 23.6 | 2.38 | 23.6 | 2.15 | 22.9 | 2.26 | 23.4 | 2.13 | 23.5 | 2.19 | 23.3 | 2.03 | 22.6 | 2.09 |
| 19.4 | 1.97 | 19.3 | 2.04 | 19.3 | 2.09 | 19.4 | 2.24 | 19.5 | 2.00 | 19.0 | 2.12 | 19.4 | 1.99 | 19.3 | 2.04 | 19.2 | 1.89 | 18.7 | 1.94 |
| 15.5 | 1.83 | 15.4 | 1.86 | 15.6 | 1.93 | 15.5 | 2.06 | 15.4 | 1.84 | 15.2 | 1.95 | 15.4 | 1.82 | 15.7 | 1.88 | 15.4 | 1.72 | 15.3 | 1.79 |
| 11.9 | 1.64 | 11.8 | 1.68 | 11.7 | 1.73 | 11.8 | 1.89 | 11.7 | 1.66 | 11.5 | 1.76 | 11.7 | 1.64 | 11.7 | 1.69 | 11.7 | 1.54 | 11.4 | 1.60 |
| 8.46 | 1.45 | 8.37 | 1.49 | 8.26 | 1.52 | 8.32 | 1.67 | 8.30 | 1.45 | 8.15 | 1.56 | 8.28 | 1.45 | 8.33 | 1.48 | 8.27 | 1.35 | 8.20 | 1.41 |
| 5.08 | 1.17 | 5.19 | 1.22 | 5.03 | 1.26 | 5.07 | 1.41 | 5.09 | 1.17 | 5.00 | 1.30 | 5.16 | 1.17 | 5.15 | 1.23 | 5.07 | 1.07 | 5.09 | 1.15 |
| 3.43 | 1.07 | 3.56 | 1.13 | 3.44 | 1.17 | 3.43 | 1.34 | 3.46 | 1.08 | 3.34 | 1.19 | 3.46 | 1.08 | 3.48 | 1.11 | 3.42 | 0.98 | 3.32 | 1.03 |
| 2.72 | 0.98 | 2.81 | 1.04 | 2.74 | 1.10 | 2.74 | 1.25 | 2.75 | 1.01 | 2.68 | 1.11 | 2.73 | 0.99 | 2.77 | 1.04 | 2.77 | 0.92 | 2.68 | 0.96 |
| 2.37 | 0.97 | 2.42 | 1.01 | 2.38 | 1.07 | 2.40 | 1.24 | 2.38 | 0.97 | 2.34 | 1.07 | 2.42 | 0.96 | 2.38 | 1.00 | 2.39 | 0.88 | 2.34 | 0.93 |
| 2.05 | 0.93 | 2.09 | 0.97 | 2.03 | 1.04 | 2.03 | 1.21 | 2.05 | 0.93 | 2.01 | 1.04 | 2.04 | 0.91 | 2.04 | 0.96 | 2.03 | 0.84 | 1.99 | 0.90 |
| 1.70 | 0.88 | 1.73 | 0.91 | 1.69 | 1.04 | 1.70 | 1.14 | 1.70 | 0.87 | 1.68 | 0.99 | 1.71 | 0.87 | 1.71 | 0.93 | 1.70 | 0.79 | 1.68 | 0.83 |

A more detailed analysis of this behaviour is given in the companion paper by Soliman & Sims (1992, this issue, pp. 229–235).

The experimental data corresponding to the condition of dual discharge are provided in table 2. In order to illustrate the influence of $Fr_2$ on $h/d$, the segment of the results corresponding to $L/d = 1.5$ is presented in figure 4. This figure shows that $h/d$ increases as $Fr_2$ increases for all values of $Fr_1$. Similarly to the case of gas pull-through (Parrott *et al.* 1991), the present results show that the percentage increase in $h/d$ at any given value of $Fr_2$ is much more pronounced at low $Fr_1$ and it drops monotonically as $Fr_1$ increases. For example, with $L/d = 1.5$ and $Fr_2 = 32.1$, the value of $h/d$ at $Fr_1 \approx 1.7$ is about 43% higher than the value measured with single discharge, while at $Fr_1 \approx 27.5$, the increase is only about 14%.

By examining the data in table 2, it is clear that the influence of the second discharge is enhanced as the distance between the orifices is decreased. This is illustrated in figure 5 for $Fr_2 = 31.5 \pm 0.6$ with the data labelled $L/d = \infty$ corresponding to the condition of single discharge. Figure 5 shows that for the range of parameters covered in this study, the flow through the second orifice has a small effect on $h/d$ for $L/d > 4$. However, for lower values of $L/d$, the influence can be significant depending on the magnitudes of $Fr_1$ and $Fr_2$.

## 3. THEORY AND COMPARISONS

### *3.1. Model development*

In this analysis, Craya's (1949) approach for a single orifice is extended to the present case of two orifices. The configuration under consideration is shown in figure 6. Stratified layers of two immiscible fluids with densities $\rho$ and $\rho + \Delta\rho$ are contained in a large reservoir with two side orifices separated by a vertical distance $L$. The interface between the stationary heavier fluid and the lighter fluid is deflected upwards in the area near the wall due to the motion in the lighter fluid. This motion is caused by the discharge through the orifices, which are simulated here as point sinks with strengths $n_1$ and $n_2$. The relationship between the strength $n$ and the mass flow rate $\dot{m}$ for either sink is given by (Milne-Thomson 1968)

$$n = \frac{\dot{m}}{(2\pi\rho)}. \qquad [9]$$

The effects of viscosity and surface tension are assumed to be negligible. Within the lighter fluid, steady, incompressible, potential flow is assumed. Equilibrium of the interface is, therefore,

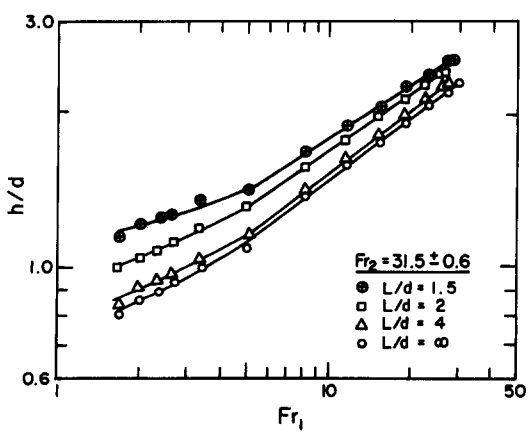


Figure 5. The influence of $L/d$ during dual discharge for $Fr_2 = 31.5$.

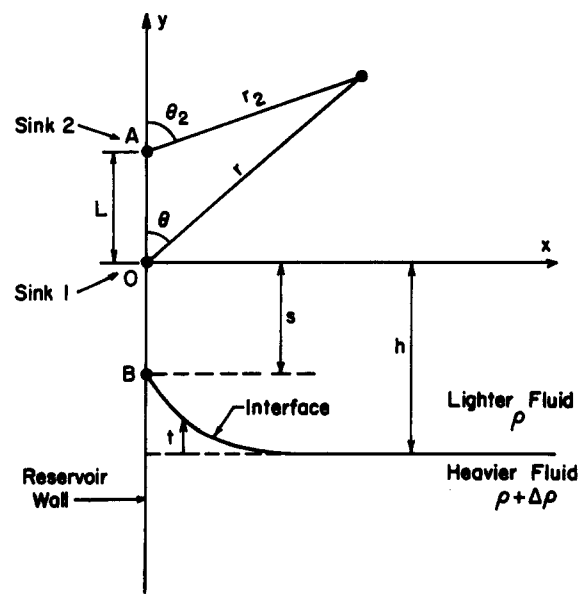


Figure 6. Theoretical parameters and the coordinate system.

controlled by a balance between inertia and gravity forces, which results in the following relation (Craya 1949; Soliman & Sims 1992):

$$\frac{V^2}{2} = \frac{\Delta\rho}{\rho} gt, \qquad [10]$$

where $V$ is the local velocity along the interface and $t$ is the local deflection measured from the flat interface. Point B (shown in figure 6) is the linking point between the interface and the reservoir wall. This point corresponds to $t = h - s$, where $s$ is the distance between the lower sink and the tip of the deflected interface; therefore

$$\frac{V_B^2}{2} = \frac{\Delta\rho}{\rho} g(h - s). \qquad [11]$$

In developing the velocity field in the lighter fluid, the presence of the heavier stationary fluid is ignored. The three-dimensional flow of the lighter fluid is axisymmetric around the $y$-axis which passes through the two sinks. Therefore, some analogy exists with the case of two-dimensional flow, thereby allowing the introduction of a stream function and a velocity potential. Following Milne-Thomson (1968), the potential function in the $x$–$y$ plane, which is perpendicular to the reservoir wall, is given by

$$\phi = -\frac{n_1}{r} - \frac{n_2}{r_2}, \qquad [12]$$

where $\phi$ is the potential function, $r$ is the radial distance from the origin O (lower sink) and $r_2$ is the radial distance from point A (upper sink). Using simple trigonometry, [12] can be formulated as

$$\phi = -\frac{n_1}{r} - \frac{n_2}{\sqrt{r^2 + L^2 - 2rL\cos\theta}}, \qquad [13]$$

where the angle $\theta$ is defined in figure 6. The radial velocity $V_r$ at any point in the $x$–$y$ plane can be obtained from

$$V_r = -\frac{\partial\phi}{\partial r} = -\frac{n_1}{r^2} - \frac{n_2(r - L\cos\theta)}{(r^2 + L^2 - 2rL\cos\theta)^{3/2}}. \qquad [14]$$

Our main interest is to determine the velocity $V_y$ along the reservoir wall beneath the lower sink ($x = 0$ and $y < 0$). In that region, the relations $\theta = \pi$, $r = -y$ and $V_y = -V_r$ are in effect. Therefore, for $x = 0$ and $y < 0$,

$$V_y = \frac{n_1}{y^2} + \frac{n_2}{(y - L)^2}. \qquad [15]$$

At linking point B, where $y = -s$, we have

$$\frac{V_B^2}{2} = \frac{1}{2}\left[\frac{n_1}{s^2} + \frac{n_2}{(s + L)^2}\right]^2. \qquad [16]$$

Following Craya (1949), the onset of liquid entrainment is characterized by the condition where values of $V_B^2/2$ given by [11] and [16] are equal, and their first derivative with respect to $s$ are also equal. Thus, the onset of the phenomenon is given by

$$\frac{2g\,\Delta\rho}{\rho}(h - s) = \left[\frac{n_1}{s^2} + \frac{n_2}{(s + L)^2}\right]^2 \qquad [17]$$

and

$$\frac{g\,\Delta\rho}{2\rho} = \left[\frac{n_1}{s^2} + \frac{n_2}{(s + L)^2}\right]\left[\frac{n_1}{s^3} + \frac{n_2}{(s + L)^3}\right]. \qquad [18]$$

Equations [17] and [18] can be non-dimensionalized using [9] to take these final forms:

$$\left[\frac{\mathrm{Fr}_1^{*}}{S^2}+\frac{\mathrm{Fr}_2^{*}}{(1+S)^2}\right]\left[\frac{\mathrm{Fr}_1^{*}}{S^3}+\frac{\mathrm{Fr}_2^{*}}{(1+S)^3}\right]=32, \qquad [19]$$

and

$$H=S+\frac{1}{4}\left[\frac{\dfrac{\mathrm{Fr}_1^{*}}{S^2}+\dfrac{\mathrm{Fr}_2^{*}}{(1+S)^2}}{\dfrac{\mathrm{Fr}_1^{*}}{S^3}+\dfrac{\mathrm{Fr}_2^{*}}{(1+S)^3}}\right], \qquad [20]$$

where

$$\mathrm{Fr}^{*}=\frac{\left(\dfrac{4}{\pi}\right)\dot{m}}{\sqrt{g\rho\,\Delta\rho\,L^5}}, \qquad [21a]$$

$$H=\frac{h}{L} \qquad [21b]$$

and

$$S=\frac{s}{L}. \qquad [21c]$$

For any given values of $\mathrm{Fr}_1^{*}$ and $\mathrm{Fr}_2^{*}$, the corresponding values of $S$ and $H$ can be obtained from [19] and [20], respectively. Together, [19] and [20] are of the form

$$H=H(\mathrm{Fr}_1^{*},\mathrm{Fr}_2^{*}) \qquad [22a]$$

and

$$S=S\ (\mathrm{Fr}_1^{*},\ \mathrm{Fr}_2^{*}). \qquad [22b]$$

The functional relation [22a] and the dimensionless groups involved ($H$, $\mathrm{Fr}_1^{*}$, $\mathrm{Fr}_2^{*}$) can also be obtained from a simple dimensional analysis neglecting the effect of diameter. However, the present theory is necessary for determining the mathematical relations among the variables given by [19] and [20]. Needless to say [22a] is a simpler form than [3], where the diameter was included as a physical quantity. Therefore, using the new dimensionless groups $H$, $S$ and $\mathrm{Fr}^{*}$ allows for a more concise way of presenting the results, as shown later. These dimensionless groups and the more conventional ones used in the experimental part are related by

$$\mathrm{Fr}=\left(\frac{L}{d}\right)^{2.5}\mathrm{Fr}^{*} \qquad [23a]$$

and

$$\frac{h}{d}=\left(\frac{L}{d}\right)H. \qquad [23b]$$

The limiting condition of a single discharge corresponds to $\mathrm{Fr}_2^{*}=0$. For this condition, [20] reduces to $s=0.8\,h$, and [19] reduces to [8], consistent with Craya's (1949) results.

### *3.2. Theoretical results*

Based on [19] and [20], computations were made in order to determine the functional relations given by [22a, b]. Figure 7 shows the variation of $H$ with $\mathrm{Fr}_1^{*}$ at different values of $\mathrm{Fr}_2^{*}$. Qualitatively, these results exhibit the same trends seen from the experimental data (figures 4 and 5). For any $\mathrm{Fr}_1^{*}$, an increase in $\mathrm{Fr}_2^{*}$ (which can be done by increasing $\mathrm{Fr}_2$ or decreasing $L/d$) results in an increase in $H$. This increase is much more pronounced (percentagewise) at low $\mathrm{Fr}_1^{*}$ than at high $\mathrm{Fr}_1^{*}$.

The present computations indicate that the dependence of $S$ on $\mathrm{Fr}_1^{*}$ and $\mathrm{Fr}_2^{*}$ is similar in form to figure 7. A more interesting way of presenting the values of $S$ is shown in figure 8, where the ratio of $S/H$ is plotted against $\mathrm{Fr}_2^{*}$ for a number of fixed values of $\mathrm{Fr}_1^{*}$. For a single discharge,

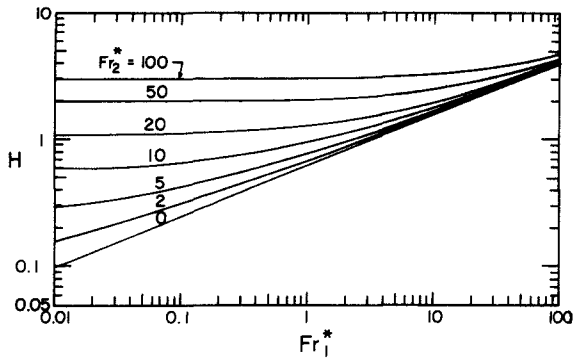


Figure 7. Theoretical correlation of the critical height.

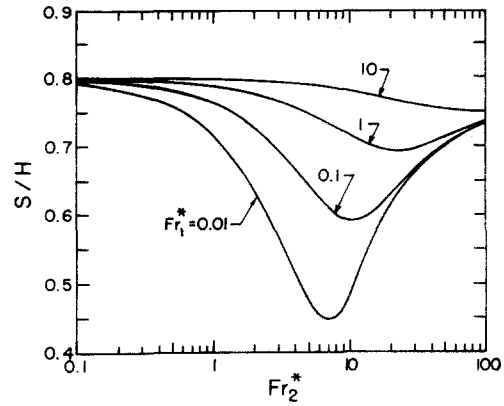


Figure 8. Variation of $S/H$ with $Fr_1^*$ and $Fr_2^*$.

the ratio $S/H = 0.8$, and this value is approached at low $Fr_2^*$ for all $Fr_1^*$. As $Fr_2^*$ increases, while $Fr_1^*$ is kept constant, $S/H$ decreases to a minimum before increasing again towards the single-discharge value. The value of $Fr_2^*$ at which $S/H$ reaches a minimum increases as $Fr_1^*$ increases. In general, the deviation from the single-discharge value decreases as $Fr_1^*$ increases.

### *3.3. Comparison between theory and experiment*

Two important questions are considered in this section. These are:

(a) Is there experimental evidence to support the contention that $H$ and Fr* are relevant dimensionless groups for the present problem? In other words, would data points of the same $Fr_1^*$ and $Fr_2^*$, but generated by different combinations of $Fr_1$, $Fr_2$ and $L/d$, have the same $H$?

(b) Can the theoretical model given by [19] and [20] reasonably predict the experimental data?

Figures 9–11 were designed to address the above questions. Each of the three figures contains two data sets with nearly the same $Fr_2^*$ but different $Fr_2$ and $L/d$. The data set corresponding to the highest $Fr_2^*$ is shown in figure 10 and the data set corresponding to the lowest $Fr_2^*$ is shown in figure 11. These figures indicate that whenever $Fr_2^*$ is close for any two sets, the data points collapse on the same line. In general, the theory overpredicts the data; however, the deviations are small (mostly under 10%) which constitutes good agreement between the theoretical predictions and the experimental results. The deviations referred to no doubt result from some combination of the simplifying assumptions adopted in the theory (e.g. negligible viscosity and surface tension, simulation of the orifices as point sinks, potential flow in the lighter fluid while ignoring the presence of the heavier fluid etc.).

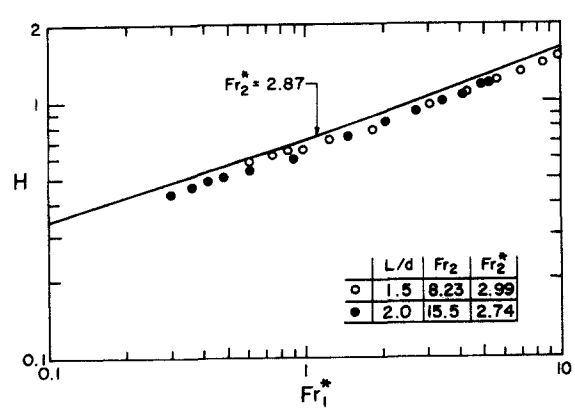


Figure 9. Comparison between theory and experiment ($Fr_2^* = 2.87$).

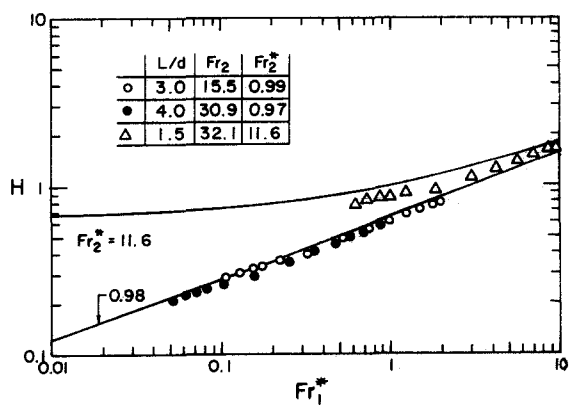


Figure 10. Comparison between theory and experiment ($Fr_2^* = 0.98$ and 11.6).

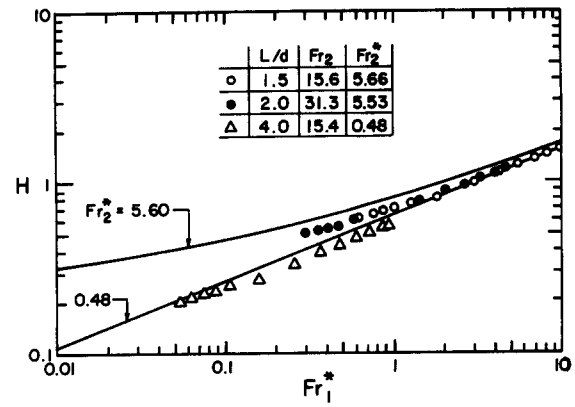


Figure 11. Comparison between theory and experiment ($Fr_2^* = 0.48$ and 5.60).

## 4. CONCLUDING REMARKS

The onset of liquid entrainment during dual discharge from large reservoirs has been investigated experimentally and theoretically. The experimental data correspond to air–water stratified layers at 310 kPa with $d = 6.35$ mm and $1.5 \leqslant L/d \leqslant 4$. Values of the critical height were measured for a wide range of discharges from the two orifices. These data indicate that the critical height increases with an increase in either discharge rate or a decrease in $L/d$. Within the present range of operating conditions, influence of the second discharge on the critical height appears to be small for $L/d \geqslant 4$.

A theoretical model has been developed by extending Craya's (1949) analysis to the present condition of dual discharge. New dimensionless groups were identified and their relevance to the phenomenon has been justified by the experimental data. As well, good agreement was found between the experimental values of the critical height and the theoretical predictions.

*Acknowledgements*—The financial support provided by the Whiteshell Laboratories (Atomic Energy of Canada Ltd) and the Natural Sciences and Engineering Research Council of Canada is gratefully acknowledged.

## REFERENCES

CRAYA, A. 1949 Theoretical research on the flow of non-homogeneous fluids. *Houille Blanche* **4**, 44–55.

CROWLEY, C. J. & ROTHE, P. H. 1981 Flow visualization and break mass measurements in small break separate effect experiments. Presented at the *ANS Special. Mtg on Small Break Loss of Coolant Accident Analyses in LWRs*, Monterey, CA.

MICAELLI, J. C. & MEMPONTEIL, A. 1989 Two phase flow behaviour in a tee junction: the CATHARE model. In *Proc. 4th Int. Top. Mtg on Nuclear Reactor Thermal-hydraulics*, Karlsruhe, Germany, Vol. 2, pp. 1024–1030.

MILNE-THOMSON, L. M. 1968 *Theoretical Hydrodynamics*, 5th edn. Macmillan, London.

PARROTT, S. D., SOLIMAN, H. M., SIMS, G. E. & KRISHNAN, V. S. 1991 Experiments on the onset of gas pull-through during dual discharge from a reservoir. *Int. J. Multiphase Flow* **17**, 119–129.

SCHROCK, V. E., REVANKAR, S. T., MANNHEIMER, R., WANG, C.-H. & JIA, D. 1986 Steam–water critical flow through small pipes from stratified upstream regions. In *Proc. 8th Int. Heat Transfer Conf.*, San Francisco, CA, Vol. 5, pp. 2307–2311.

SMOGLIE, C. & REIMANN, J. 1986 Two-phase flow through small branches in a horizontal pipe with stratified flow. *Int. J. Multiphase Flow* **12**, 609–625.

SMOGLIE, C., REIMANN, J. & MULLER, U. 1987 Two-phase flow through small breaks in a horizontal pipe with stratified flow. *Nucl. Engng Des.* **99**, 117–130.

SOLIMAN, H. M. & SIMS, G. E. 1992 Theoretical analysis of the onset of liquid entrainment for orifices of finite diameter. *Int. J. Multiphase Flow* **18**, 229–235.

ZUBER, N. 1980 Problems in modeling of small break LOCA. Report NUREG-0724.